 CMES, vol.48, no.1, pp.83-105, 2009

Effects of the Rayleigh Number and the Aspect Ratio on 2D Natural Convection Flows

Alfredo Nicolás[1], Blanca Bermúdez[2] and Elsa Báez[3]

Abstract: Numerical results of natural convection flows in two-dimensional cavities, filled with air, are presented to study the effects on the characteristics of the flows as some parameters vary: the Rayleigh number Ra and the aspect ratio A of the cavity. This kind of thermal flows may be modeled by the unsteady Boussinesq approximation in stream function-vorticity variables. The results are obtained with a simple numerical scheme, previously reported for isothermal/mixed convection flows, based mainly on a fixed point iterative process applied to the non-linear elliptic system that results after time discretization. The evolution of the flows, mainly flows converging to a steady state, depends on the variation of the parameters in the range: $10^5 \leq Ra \leq 10^7$, $\frac{1}{4} \leq A \leq 4$. The study is complemented with the corresponding heat transfer through the Nusselt numbers as well as the time T_{ss} when the steady state of the flow is reached; in connection with T_{ss}, the flow at different times less than T_{ss} is reported for $Ra = 10^6$ with $A = 1$, some findings become into light about transient phenomenon. The validation of the results is given through mesh size and time-step independence studies complemented with the corresponding independence of some characteristics of the flow; then, the validation process is not depending on the comparison with other works using different dimensionless forms.

Keywords: unsteady Boussinesq approximation, Rayleigh number, aspect ratio, heat transfer

1 Introduction

The study on natural convection flows in inclosures is usually divided into two main classes, those heated from below and those heated from the side; the lat-

[1] Depto. Matemáticas, 3er. Piso Ed. Diego Bricio, UAM-Iztapalapa, 09340 México D.F. México, e-mail: anc@xanum.uam.mx

[2] Facultad de C. de la Computación, BUAP, Pue., México

[3] Depto. Matemáticas Aplicadas y Sistemas, UAM-C; 01120 México D.F., México, *correspondence to*: Alfredo Nicolás

ter class being the differentially heated cavity. This configuration models many engineering applications; to name a few: energy storage systems, nuclear reactor insulation, ventilation of buildings, and cooling of electronic devices; recent applications can also be found in greenhouses' design, Rico-García et al. (2008). It has then, considerable practical and theoretical importance becoming a classical problem in the convective heat transfer and fluid mechanics literature, Le Quéré and Alziary Roquefort (1985).

The unsteady Boussinesq approximation for viscous incompressible fluid flow thermally coupled in a gravitational system, from which the natural convection phenomenon is a particular case, is based on the fact that temperature variations are small enough to imply that density variations are negligible except for the buoyancy force in the momentum equation, leading to an incompressible structure. That is to say, considering the density ρ as constant except in the term $\rho\mathbf{g}$, with $\mathbf{g}$ the gravitational force and ρ, from the state equation, given linearly by $\rho = \rho_0[1-\beta(T-T_0)]$, where T is the temperature and $\beta = -\frac{1}{\rho_0}(\frac{\partial\rho}{\partial T})_P$ the constant coefficient of thermal expansion, the density change due to changes in pressure is neglected, ρ_0 and T_0 denote reference density and temperature respectively; the dissipation of mechanical energy is neglected; and other fluid properties, such as dynamic viscosity μ, the thermal diffusivity η, and the specific heat c_p are assumed to be constants; Gunzburger (1989), Landau and Lifshitz (1989). Moreover, in this work the $2D$ formulation in stream function and vorticity variables is considered; then, the incompressibility condition is automatically satisfied and the pressure is avoided to be computed.

Concerning the numerical method, after a convenient second order time discretization, a non-linear system of elliptic equations is obtained which is solved through an iterative fixed point process. Then, at each iteration, uncoupled, well-conditioned, symmetric linear elliptic problems have to be solved for which very efficient solvers exist regardless of the space discretization. This numerical method, previously reported in Nicolás and Bermúdez (2005) for mixed convection and in Baéz and Nicolás (2006) for natural convection in tilted cavities, has turned out to be robust enough to study the effects on the characteristics of natural convection flows in two-dimensional cavities, filled with air, as some parameters vary: the Rayleigh number Ra and the aspect ratio A of the cavity (A=ratio of the height to the width). Actually, the following facts reinforce the robustness of the numerical method: it can handle flows like in Arefmanesh et al. (2008) where a meshless local Petrov-Galerking (MLPG) method is used, some of them in connection with mixed convection just mentioned, Nicolás and Bermúdez (2005); it works well for moderate and high Reynolds numbers when is restricted to the isothermal case, Nicolás and Bermúdez (2004) as well as, with some modification, for the formulation in velocity and vor-

ticity variables, Nicolás and Bermúdez (2007); it can also be adapted to deal with Darcy natural convection flows in porous media, as in Báez and Nicolás (2006), to obtain results that can agree with those in Kosec and Ŝarler (2008) where a mesh-free Local Radial Basis Function Collocation Method (LRBFCM) approach is used in the primitive variables formulation. To solve the mathematical system that involves elliptic and parabolic problems the spatial discretization process involves finite difference uniform meshes, until the boundary, then none adaptive refinement is required as in Bourantas (2009) where mesh-free methods based on point collocation (PC) techniques are used. Among natural convection problems involving more complex phenomenon, solid-liquid phase change in a more complex geometry, the one in Avila and Solorio (2009) can be mentioned. To have efficient solvers for problems, as the one presented here, can be the basis to handle inverse problems, like the one for a simpler conduction problem that is stated in Marin (2008).

It can be pointed out that to solve nonlinear problems, of which the one that is solved in this work is a particular one, recent Meshless methods like meshless local Petrov-Galerking (MLPG) belong to one of the most progressively developed part of the computational mechanics and they are increasingly applied to many fields of engineering and sciences. Actually, the MLPG methods were first published by Atluri and Zhu (1998). Since then, this kind of methodology has been continuously being applied in other kind of nonlinear problems using the Moving Least Square (MLS) approximation, radial basis function (RBF), partition of unity (PU) as trial functions, point collocation and meshless finite volume methods, the local boundary integral equation (LBIE) method, and Galerkin techniques as well as local weak-forms; to name some works on this direction: Li and Atluri (2008), Atluri et al. (2006), (1) and (3). Moreover, a more complete presentation of these methods, including several applications and more general nonlinear problems, can be found in Atluri et al. (2009), Atluri (2005), Atluri (2004), Atluri and Shen (2002).

To be specific, the goal of this paper is to undertake this study as the parameters mentioned vary in the range: $10^5 \leq Ra \leq 10^7$ and $\frac{1}{4} \leq A \leq 4$. The study is complemented with the corresponding heat transfer through the Nusselt numbers, local and global. The time T_{ss} when the steady state of the flow is reached is also reported, an issue that is not usually considered when the unsteady problem is solved; in this way, the time length of the transient stage is determined. For $Ra = 10^6$ and $A = 1$, with T_{ss} known, the flow at different times less than T_{ss} is reported; with this example we are given the analogous situation given in Saeid and Pop (2004) for porous media flows, on this regard some findings become into light about transient phenomenon.

The results, mainly flows converging to a steady state, are accompanied with a

validation process through mesh size and time-step independence studies complemented with the corresponding independence of some parameters of the flow; another source of self-validation is given by flows at different times before T_{ss} is reached. Then, the results are not depending on the comparison with other works that use different dimensionless forms. However, a comparison will be made with some works, among others: De Vahl Davis (1983), Le Quéré and Alziary Roquefort (1985). The first one in connection with $Ra = 10^5$, 10^6, and the second one with $Ra = 10^7$; all of them with $A = 1$, and all these results also agree with those in Ho-Minh et al. (2009), where the unsteady problem in stream function and vorticity variables, like here, is solved using a Galerkin-RBF approach. It should be noted that in this work besides flows in the square cavity, $A = 1$, attention is also focussed on concentric annulus flows while ours on $A = 1$, $A \neq 1$ and on the corresponding heat transfer; another difference among both works is the way to build the boundary condition for the vorticity, concerning rectangular cavities.

Hereafter, the paper is organized in sections as follows: 2. Mathematical model and numerical method, 3. Results and discussion, 4. Conclusions.

2 Mathematical model and numerical method

Let $\Omega \subset R^N$ $(N = 2,3)$ be the region of the flow of a unsteady thermal viscous incompressible fluid flow, and let Γ its boundary. Under the well known hypothesis of the Boussinesq approximation, this kind of flows is modeled by the dimensionless system

$$\begin{array}{lll} \mathbf{u}_t - \nabla^2\mathbf{u} + \nabla p + (\mathbf{u}\cdot\nabla)\mathbf{u} & = \frac{Ra}{Pr}\theta\mathbf{e} & (a) \\ \nabla\cdot\mathbf{u} & = 0 & (b) \\ \theta_t - \frac{1}{Pr}\nabla^2\theta + \mathbf{u}\cdot\nabla\theta & = 0 & (c) \end{array} \tag{1}$$

in Ω, $t > 0$; where $\mathbf{u}$, p and θ are the velocity, pressure, and temperature of the flow respectively, $\mathbf{e}$ is the unitary vector in the gravitational direction. The dimensionless parameters Ra and Pr are the Rayleigh and Prandtl numbers given respectively by $Ra = \frac{\beta l^3 \kappa g \rho_0^2}{\mu^3 c_p}(T_l - T_0)$, $Pr = \kappa/\mu c_p$, where T_0 and T_1 are reference temperatures, $T_0 < T_1$, which may be the temperature of the lateral sides when the flow region is a rectangular cavity, l is the reference length of the region, ν $(=\frac{\mu}{\rho_o})$ the cinematic viscosity, and g the gravitational constant. The dimensionless temperature θ is given by $\theta = \frac{T-T_0}{T_l-T_0}$. The system must be supplemented with initial conditions $\mathbf{u}(\mathbf{x},0) = \mathbf{u}_0(\mathbf{x})$ and $\theta(\mathbf{x},0) = \theta_0(\mathbf{x})$ in Ω; and boundary conditions, for instance $\mathbf{u} = \mathbf{f}$ and $B\theta = 0$ on Γ, $t \geq 0$, where B is a temperature boundary operator that can involve Dirichlet, Neumann or mixed type boundary conditions.

Restricting the equations (1a-c) to a bi-dimensional region Ω, taking the curl in

both sides of equation $(1a)$ and taking into account

$$u_1 = \frac{\partial \psi}{\partial y}, \quad u_2 = -\frac{\partial \psi}{\partial x}, \tag{2}$$

which follow from $(1b)$, with ψ the stream function and $(u_1, u_2) = \mathbf{u}$; the component in the direction $\mathbf{k} = (0,0,1)$ gives the scalar system

$$\begin{array}{lll} \nabla^2 \psi & = -\omega & (a) \\ \omega_t - \nabla^2 \omega + \mathbf{u} \cdot \nabla \omega & = \frac{Ra}{Pr} \frac{\partial \theta}{\partial x} & (b) \\ \theta_t - \gamma \nabla^2 \theta + \mathbf{u} \cdot \nabla \theta & = 0 & (c) \end{array} \tag{3}$$

in Ω, $t > 0$; where $\gamma = 1/Pr$ and ω is the vorticity which, from $\omega \mathbf{k} = \nabla \times \mathbf{u} = -\nabla^2 \psi \mathbf{k}$, gives $(3a)$ and $\omega = \frac{\partial u_2}{\partial x} - \frac{\partial u_1}{\partial y}$ as well. Then, system (3) turns out to be the Boussinesq approximation in stream function and vorticity variables. The incompressibility condition $(1b)$, by (2), is automatically satisfied and the pressure p has been eliminated.

This work is concerned with natural convection in rectangular cavities, then the equations are set in $\Omega = (0,a) \times (0,b)$; $a > 0$, $b > 0$. To construct the boundary condition for ω, which is not a trivial task to deal with, various alternatives have been proposed, see for instance Peyret and Taylor (1983). Here the alternative in Nicolás and Bermúdez (2004), extended to natural convection problems in rectangular cavities, is used: by Taylor expansion of ψ on the boundary and using $(3a)$, the following $O(h_x^2)$ (the first two) and $O(h_y^2)$ (the last two) relations are obtained

$$\begin{aligned} \omega(0,y,t) &= -\frac{1}{2h_x^2}[8\psi(h_x,y,t) - \psi(2h_x,y,t)] \\ \omega(a,y,t) &= -\frac{1}{2h_x^2}[8\psi(a-h_x,y,t) - \psi(a-2h_x,y,t)] \\ \omega(x,0,t) &= -\frac{1}{2h_y^2}[8\psi(x,h_y,t) - \psi(x,2h_y,t)] \\ \omega(x,b,t) &= -\frac{1}{2h_y^2}[8\psi(x,b-h_y,t) - \psi(x,b-2h_y,t)] \end{aligned} \tag{4}$$

where h_x and h_y denote the size of the spatial discretization in X and Y directions. It should be observed that the boundary values for ω are given by values in Ω and $t > 0$, still unknown, of the stream function ψ. This problem will be solved within a fixed point iterative process.

The local Nusselt number Nu measures the heat transfer at each point on the wall where the temperature is specified and the global Nusselt number $\overline{Nu}$ measures the

average heat transfer on the wall. These non-dimensional parameters are defined by:

local Nusselt number,

$$Nu(x) = -\frac{\partial\theta}{\partial y}|_{y=0,b} \text{ or } Nu(y) = -\frac{\partial\theta}{\partial x}|_{x=0,a};$$

global Nusselt number,

$$\overline{Nu}\,|_{y=0,b} = \frac{1}{A}\int_0^a Nu(x)dx \text{ or}$$
$$\overline{Nu}\,|_{x=0,a} = \frac{1}{A}\int_0^b Nu(y)dy.$$

Once the time derivatives of ω and θ in (3) are approximated by the second order approximation

$$f_t(\mathbf{x},(n+1)\Delta t) \approx \frac{3f^{n+1}-4f^n+f^{n-1}}{2\Delta t} \tag{5}$$

where $n \geq 1$, $\mathbf{x}\ \varepsilon\ \Omega$, $\Delta t > 0$ is the time step, and $f^r \approx f(\mathbf{x}, r\Delta t)$, at each time level $t = (n+1)\Delta t$ the semi-discrete system, in Ω, with its corresponding boundary conditions on Γ, reads

$$\begin{aligned}
&\nabla^2\psi^{n+1} = -\omega^{n+1}, && \psi^{n+1}|_\Gamma = 0\\
&\alpha\omega^{n+1} - \nabla^2\omega^{n+1} + \mathbf{u}^{n+1}\cdot\nabla\omega^{n+1} = \tfrac{R_a}{Pr}(\tfrac{\partial\theta}{\partial x})^{n+1} + f_\omega, && \omega^{n+1}|_\Gamma = \omega_{bc}^{n+1}\\
&\alpha\theta^{n+1} - \gamma\nabla^2\theta^{n+1} + \mathbf{u}^{\mathbf{n+1}}\cdot\nabla\theta^{n+1} = f_\theta, && B\theta^{n+1}|_\Gamma = 0,
\end{aligned} \tag{6}$$

where $\alpha = \frac{3}{2\Delta t}$, $f_\omega = \frac{4\omega^n-\omega^{n-1}}{2\Delta t}$, and $f_\theta = \frac{4\theta^n-\theta^{n-1}}{2\Delta t}$; ω_{bc} denotes the boundary condition of ω given in (4) and the components u_1 and u_2 of $\mathbf{u}$, in terms of ψ, are given by (2). After renaming $(\psi^{n+1}, \omega^{n+1}, \theta^{n+1})$ by (ψ, ω, θ), a non-linear elliptic system of the following form is obtained

$$\begin{aligned}
&\nabla^2\psi = -\omega, && \psi|_\Gamma = 0 && (a)\\
&\alpha\omega - \nabla^2\omega + \mathbf{u}\cdot\nabla\omega = \tfrac{Ra}{Pr}\tfrac{\partial\theta}{\partial x} + f_\omega, && \omega|_\Gamma = \omega_{bc} && (b)\\
&\alpha\theta - \gamma\nabla^2\theta + \mathbf{u}\cdot\nabla\theta = f_\theta,\ B\theta|_\Gamma = 0. && && (c)
\end{aligned} \tag{7}$$

To obtain $(\omega^1, \theta^1, \psi^1)$ in (6), a first order approximation for the time derivatives may be applied through a subsequence with a smaller time step; a stationary system of the form (7) is also obtained.

Denoting

$$R_\omega(\omega,\psi) \equiv \alpha\omega - \nabla^2\omega + \mathbf{u}\cdot\nabla\omega - \frac{Ra}{Pr}\frac{\partial\theta}{\partial x} - f_\omega,$$

$R_\theta(\theta,\psi) \equiv \alpha\theta - \gamma\nabla^2\theta + \mathbf{u}\cdot\nabla\theta - f_\theta.$

Then, system (7) is equivalent, in Ω, to

$$\begin{array}{lcll} \nabla^2\psi & = -\omega, & \psi|_\Gamma = 0 \\ R_\theta(\theta,\psi) & = & 0, \quad B\theta|_\Gamma = 0 \\ R_\omega(\omega,\psi) & = & 0, \quad \omega|_\Gamma = \omega_{bc}. \end{array} \tag{8}$$

To solve (8), at each time level $(n+1)\Delta t$, the following fixed point iterative process is applied, in Ω,

With $\{\theta^0,\omega^0\} = \{\theta^n,\omega^n\}$ *given, solve until convergence on* θ *and* ω

$$\begin{array}{l} \nabla^2\psi^{m+1} = -\omega^m, \quad \psi^{m+1}|_\Gamma = 0, \\ \theta^{m+1} = \theta^m - \rho_\theta(\alpha I - \gamma\nabla^2)^{-1}R_\theta(\theta^m,\psi^{m+1}), \\ B\theta^{m+1}|_\Gamma = 0, \quad \rho_\theta > 0, \\ \omega^{m+1} = \omega^m - \rho_\omega(\alpha I - \nabla^2)^{-1}R_\omega(\omega^m,\psi^{m+1}), \\ \omega^{m+1}|_\Gamma = \omega_{bc}^{m+1}, \quad \rho_\omega > 0 \end{array} \tag{9}$$

and take $(\omega^{n+1},\psi^{n+1},\theta^{n+1}) = (\omega^{m+1},\psi^{m+1},\theta^{m+1})$.

It should be noted that the construction of the ω boundary condition ω_{bc} in (4), given implicitly by unknown values of ψ in Ω, is performed as part of the iterative process in (9).

Finally, system (9) is equivalent to

$$\begin{array}{l} \nabla^2\psi^{m+1} = -\omega^m, \quad \psi^{m+1}|_\Gamma = 0 \\ (\alpha I - \gamma\nabla^2)\theta^{m+1} = (\alpha I - \gamma\nabla^2)\theta^m - \rho_\theta R_\theta(\theta^m,\psi^{m+1}), \\ B\theta^{m+1}|_\Gamma = 0, \quad \rho_\theta > 0 \\ (\alpha I - \nabla^2)\omega^{m+1} = (\alpha I - \nabla^2)\omega^m - \rho_\omega R_\omega(\omega^m,\psi^{m+1}), \\ \omega^{m+1}|_\Gamma = \omega_{bc}^{m+1}, \quad \rho_\omega > 0. \end{array} \tag{10}$$

Therefore, at each iteration *three* uncoupled linear elliptic problems associated with the operators ∇^2, $\alpha I - \gamma\nabla^2$, and $\alpha I - \nabla^2$ have to be solved, in Ω.

For the space discretization of elliptic problems, like those in (10), either finite differences or finite elements may be used, as far as rectangular domains are concerned; in either case efficient solvers exist. For the finite element case, variational formulations have to be chosen and then restrict them to finite dimensional finite elements spaces, like those in Gunzburger (1989) and Glowinski (2003). For the specific results in the next Section, the second order approximation of the Fishpack solver, Adams et al. (1980), is used. Then, such second order approximation

in space combined with the second order approximation in (5) for the first derivatives in time, the approximation with second order central differences at the interior points, and with (5) on the boundary, for all the first space derivatives, including those that appear in the local Nusselt number $Nu(y)$, and de second order trapezoidal rule to calculate the global Nusselt number $\overline{Nu}$ imply that the whole discrete problem relies on second order discretizations only.

3 Results and discussion

The numerical experiments take place in rectangular cavities $\Omega = (0,a) \times (0,b)$; a, $b > 0$. For natural convection all the walls of the cavity are solid and fixed, then, by viscosity, the boundary condition for $\mathbf{u}$ is $\mathbf{0}$ everywhere on Γ, by (2) ψ is constant and this constant can be chosen to be zero. The boundary condition for ω, as commented before, is given by (4) whereas the one for θ, given implicitly in the boundary operator B, is

$$\begin{cases} \theta = 1 & on\ \Gamma|_{x=0}, \\ \theta = 0 & on\ \Gamma|_{x=a} \\ \frac{\partial \theta}{\partial n} = 0 & on\ \Gamma|_{y=0,b}, \end{cases}$$

meaning that the horizontal walls are adiabatic and on the vertical walls the temperature is constant, and heating occurs on the left wall. In terms of the dimensionless temperature $\theta = \frac{T-T_0}{T_l-T_0}$ in $(1c)$ and $(7c)$ it can be seen that on the left wall a dimensional temperature T equals T_1 is being specified and on the right wall $T = T_0$. The cavities are supposed to be filled with air, implying that the Prandtl number Pr is given by $Pr = 0.71$; then, from hereafter the flows will be depending on the Rayleigh number Ra and on the aspect ratio A only.

Denoting by T_{ss} the time where the asymptotic, time limit, steady state of the flow is reached, T_{ss} is computed according to the point-wise discrete L_∞ absolute criterion on the closure of the cavity $\overline{\Omega}$

ψ: $||\psi^{n+1}_{hx,hy} - \psi^{n}_{hx,hy}||_\infty$, θ: $||\theta^{n+1}_{hx,hy} - \theta^{n}_{hx,hy}||_\infty$,

since, by definition, T_{ss} is the time when the solution, of the unsteady problem, does not change any more at any spatial point occupied by the fluid, Nicolás and Bermúdez (2005). We remark that so far the time T_{ss} is not usual to be reported when the unsteady problem is solved, at least not in terms of the strict definition of the steady state as we do; actually, we started to work on this topic once we heard it from Saeid and Pop (2004), for flows in porous media, and because of the work in Nicolás and Bermúdez (2005), in connection with mixed convection flows, and later on in Báez and Nicolás (2006) for porous media and homogeneous fluids.

The results, which are converged flows to a steady state, are reported through the streamlines and the isotherms; unless otherwise stated, they correspond to ten values obtained by default using Mathematica 6. For the dimensionless temperature θ such values start from 0.09 close to the cold right wall, which is 0.9 divided by 10, and then they increase a multiple integer until reach the value 0.9 close to the hot left wall; if some additional clarification were needed the values for the streamlines would be mentioned. The mesh size is denoted by (h_x, h_y) and by h only if $h_x = h_y$, and the time step by Δt; they will be indicated in each case under study.

To support that the flows are correct, mesh size and time-step independence studies are made in terms of the point-wise discrete L_∞ relative error on the closure of the cavity $\overline{\Omega}$

$$\begin{cases} \Delta t \text{ fixed}: & \frac{||f_{hx1,hy1;\Delta t} - f_{hx2,hy2;\Delta t}||_\infty}{||f_{hx1,hy1;\Delta t}||_\infty}, \\ \{h_x, h_y\} \text{fixed}: & \frac{||f_{hx,hy;\Delta t1} - f_{hx,hy;\Delta t2}||_\infty}{||f_{hx,hy;\Delta t1}||_\infty} \end{cases}$$

The study on the characteristics of the flow, as mentioned in the Introduction, considers variation of the parameters in the range: $10^5 \leq Ra \leq 10^7$, $\frac{1}{4} \leq A \leq 4$. The description of the results follows.

With $A = 1$, Figure 1 pictures the streamlines (left) and isotherms (right) of the flow for $Ra = 10^6$, Figure 2 the flow for $Ra = 10^7$, and Figure 3 the heat transfer through the local Nusselt numbers of these flows. These results are obtained with $h = \frac{1}{64}$ and $\Delta t = 0.00001$. It is worth to observe that the streamlines for $Ra = 10^7$ in Figure 2 are obtained with the contour values given by {-42, -40, -38, -35.75, -34, -31, -27, -22, -16, -12, -8, -4} which give a shape very close to the one given in Le Quéré and Alziary Roquefort (1985) with the contour values {5, 10, 15, 20, 22, 24, 26, 28, 30}, where the unsteady problem in primitive variables, with a different dimensionless form, is solved; this means that within a different scale the flow has the "same shape". It is worth to mention that the results in Figures 1 and 2 agree perfectly with the ones in Ho-Minh et al. (2009) and so does a preliminary result for $Ra = 10^8$ with $A = 1$.

To better understand the effect on the flow as Ra increases, we add that the contour values of the streamlines, by default, in Figure 1 are {-2.1,-4.2,-6.3,-8.4,-10.5,-12.6,-14.7,-16.8,-18.9,-21} going from the boundary toward the center of the cavity, which are multiple integers of -21 divided by 10, whereas the corresponding default values in Figure 2 are multiple integers of -38 divided by 10; in this latter case the main difference with the 12 values shown in Figure 2 is that the small inner cells do not appear. On the other hand, comparing the values -2.1 and -21 for $Ra = 10^6$ with -3.8 and -38 for $Ra = 10^7$ it is implied that the gradient of ψ is bigger for $Ra = 10^7$ since $\psi = 0$ on the boundary and that ψ enlarges more toward

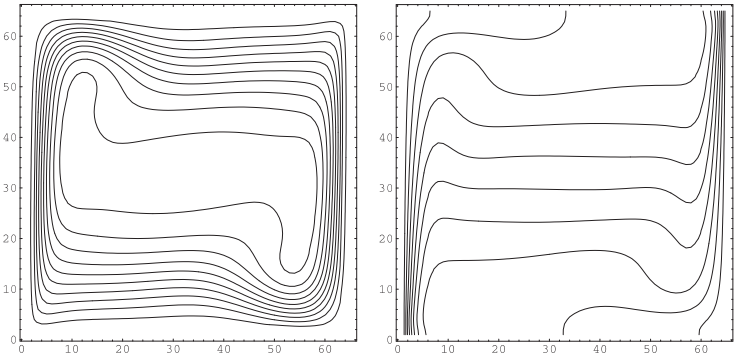

Figure 1: Streamlines and isotherms for $Ra = 10^6$ with $A = 1$: $h = \frac{1}{64}$

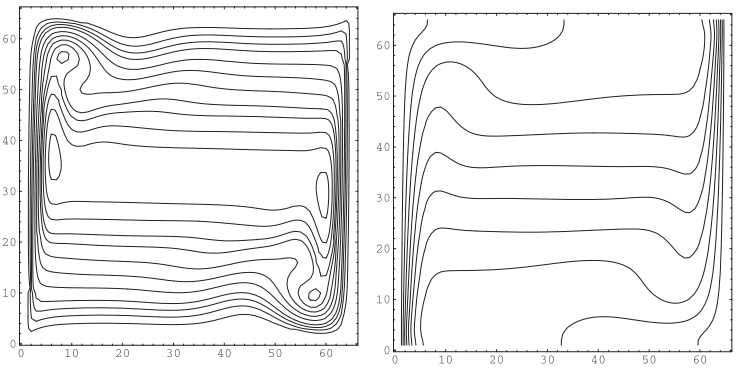

Figure 2: Streamlines and isotherms for $Ra = 10^7$ with $A = 1$: $h = \frac{1}{64}$; with Le Quéré's contour values

the center of the cavity.

For $Ra = 10^6$, the flows with $A = 2$, 3, and 4 are shown in Figure 4 through the streamlines and in Figure 5 through their isotherms; Figure 6 displays the graph of the heat transfer of the corresponding local Nusselt numbers. Subsequently, Figures 7, 8, 9, and 10 show the corresponding flows and heat transfer for the same Rayleigh number but with aspect ratios $A = \frac{1}{2}$, $\frac{1}{3}$, and $\frac{1}{4}$. The contour values of the streamlines in Figure 4, with $A = 4$, the third right one, are multiple integers of -60 divided by 10, the two inner small cells have the contour value -54 which coincides with the one of the second streamline from the center of the cavity; for the

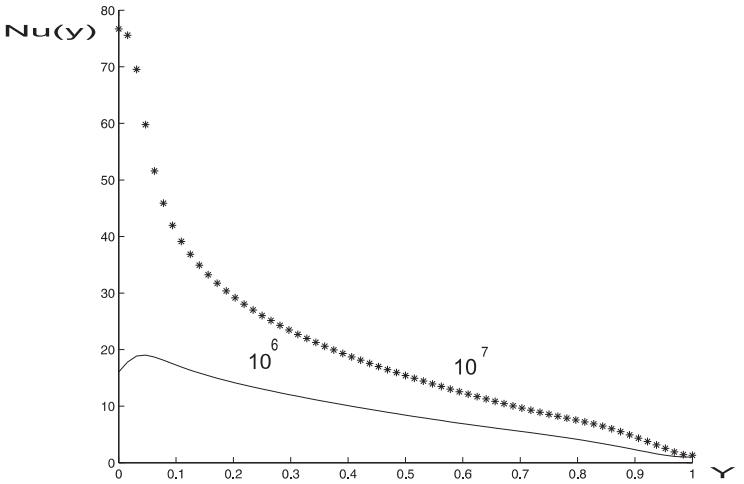

Figure 3: Local Nusselt Number for $Ra = 10^6$ and $Ra = 10^7$ with $A = 1$: $h = \frac{1}{64}$

corresponding situation in Figure 9 with $A = \frac{1}{4}$, the streamlines are multiple integers of -26 divided by 10 and the small cells along with the innermost streamline have the same contour value -26, which clearly means that the innermost streamline in the case $A = \frac{1}{3}$, Figure 8, has broken down into two pieces. All these flows with $A \neq 1$ are obtained with a uniform mesh that results increasing proportionally the number of points as the length, vertical or horizontal, is enlarged with respect to the basic mesh size $h = \frac{1}{64}$ with $A = 1$. For instance, with $A = 3$ the mesh is given by $(h_x, h_y) = (\frac{1}{64}, \frac{3}{192})$ whereas $(h_x, h_y) = (\frac{4}{256}, \frac{1}{64})$ with $A = \frac{1}{4}$; about the time step, $\Delta t = 0.00001$ works for all these cases.

A discussion on the results follows:

i) To justify the flows for $Ra = 10^6$ are correct we performed a mesh size independence study considering the meshes 1) $h = \frac{1}{32}$, 2) $h = \frac{1}{64}$, 3) $h = \frac{1}{96}$ with $A = 1$ whereas 1) $(h_x, h_y) = (\frac{1}{32}, \frac{3}{96})$, 2) $(h_x, h_y) = (\frac{1}{64}, \frac{3}{192})$, 3) $(h_x, h_y) = (\frac{1}{96}, \frac{3}{288})$ with $A = 3$; both cases with $\Delta t = 0.00001$ fixed. On this regard, Table 1 shows the discrepancies (Dis.) for the stream function ψ and temperature θ with $A = 1$ and Table 2 the corresponding ones with $A = 3$. Then, from these Tables the right flows are those obtained with the basic mesh size $h = \frac{1}{64}$

ii) The previous mesh size independence study is complemented with a time-step independence study; to this end, Table 3 displays the discrepancies with time steps $\Delta t = 0.00001$ and $\Delta t = 0.000001$ with $A = 1$ and $A = 3$, both cases with $h = \frac{1}{64}$

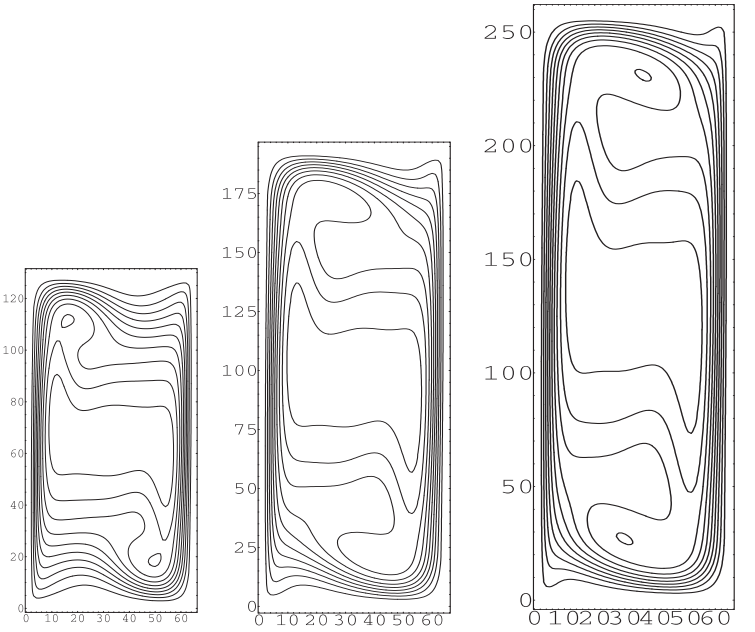

Figure 4: Streamlines for $Ra = 10^6$ with $A = 2$, 3 and 4: $h_x = \frac{1}{64}$; $h_y = \frac{2}{128}$, $h_y = \frac{3}{192}$ and $h_y = \frac{4}{256}$

Table 1: Mesh independence: $Ra = 10^6$, $A = 1$

mesh	Dis. ψ	Dis. θ
1 vs 2	2.03%	1.94%
1 vs 3	2.48%	2.22%
2 vs 3	0.45%	0.25%

Table 2: Mesh independence: $Ra = 10^6$, $A = 3$

mesh	Dis. ψ	Dis. θ
1 vs 2	5.99%	1.96%
1 vs 3	7.23%	2.23%
2 vs 3	1.24%	0.30%

fixed; it can be seen that the discrepancies are very small, and it is not necessary to use a smaller time step because it is known that for more complicate problems

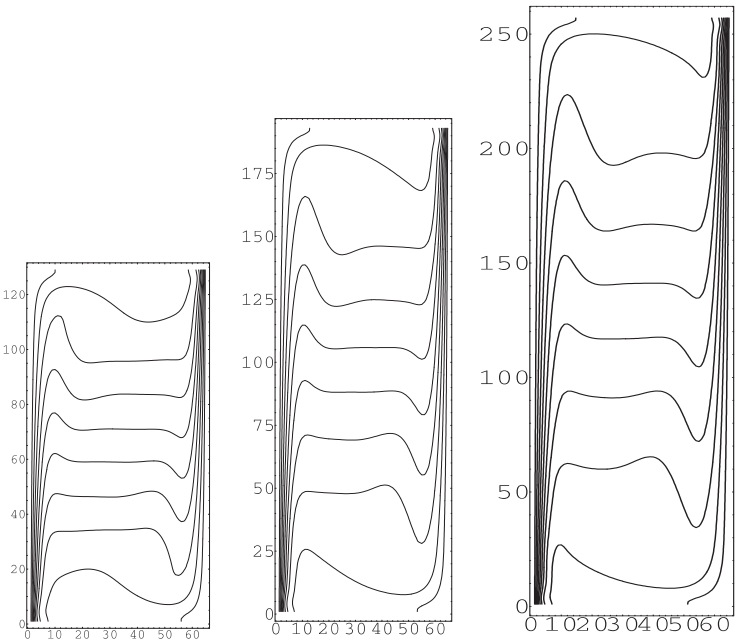

Figure 5: Isotherms for $Ra = 10^6$ with $A = 2$, 3 and 4: $h_x = \frac{1}{64}$; $h_y = \frac{2}{128}$, $h_y = \frac{3}{192}$ and $h_y = \frac{4}{256}$

like mixed convection, Nicolás and Bermúdez (2005), the discrepancies are even smaller. Then, the time step $\Delta t = 0.00001$ is enough to get the right flows, taking into consideration that with Δt bigger the method blows up.

Table 3: Time step independence: $Ra = 10^6$; $\Delta t = 10^{-5}$, 10^{-6}

A	Dis. ψ	Dis. θ
1	$5.8 \times 10^{-4}\%$	$5.2 \times 10^{-4}\%$
3	$9.9 \times 10^{-4}\%$	$7.8 \times 10^{-4}\%$

iii) To reinforce the correctness of the flows, with such mesh size and Δt, in Tables 4 and 5 various quantities are displayed with the finer meshes generated by $h = \frac{1}{64}$ and $h = \frac{1}{96}$. Those quantities are: the minimum value of the stream function ψ^{min} (which equivalently can be given as the maximum value of $|\psi|$), the global Nusselt number $\overline{Nu}$ which measures the average heat transfer from the hot wall (left one) into the fluid, and the time T_{ss} when the steady state of the flow is reached; the

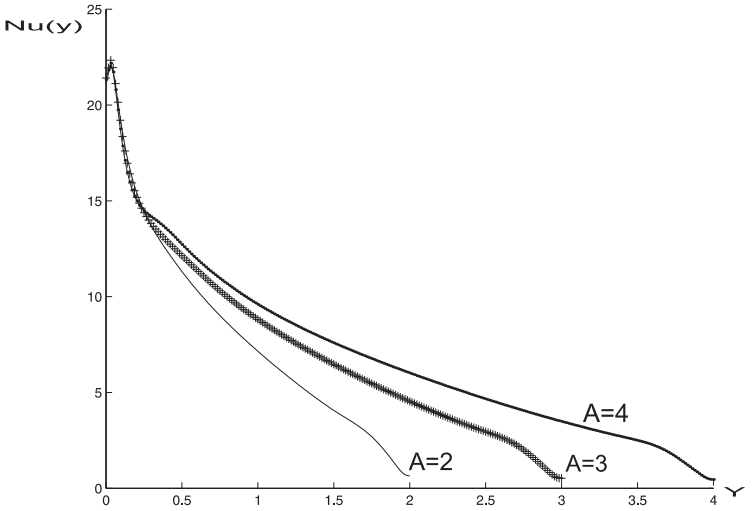

Figure 6: Local Nusselt Number for $Ra = 10^6$: $A = 2$, 3 and 4

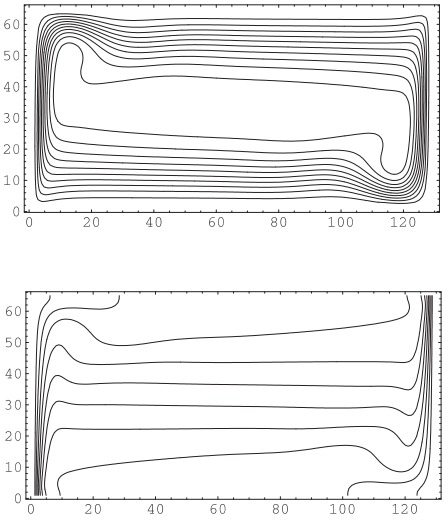

Figure 7: Streamlines(above) and isotherms(below) for $Ra = 10^6$ with $A = \frac{1}{2}$: $h_x = \frac{2}{128}$, $h_y = \frac{1}{64}$

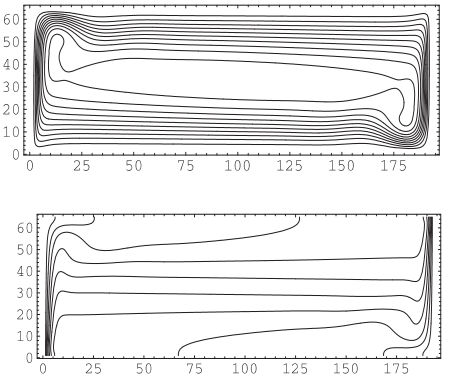

Figure 8: Streamlines(above) and isotherms(below) for $Ra = 10^6$ with $A = \frac{1}{3}$: $h_x = \frac{3}{192}$, $h_y = \frac{1}{64}$

discrepancies shown by these Tables say that no significant difference is observed with the finer mesh $h = \frac{1}{96}$. Then, under this additional criterion, the values with

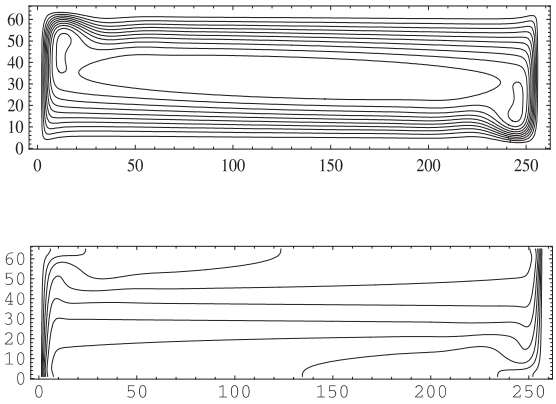

Figure 9: Streamlines(above) and isotherms(below) for $Ra = 10^6$ with $A = \frac{1}{4}$: $h_x = \frac{4}{256}$, $h_y = \frac{1}{64}$

Table 4: Ra=10^6; h=1/64, dt=0.00001: Various quantities

A	ψ^{min}	$\overline{N}u$	T_{ss}
$\frac{1}{4}$	-29.182	31.528	0.943
$\frac{1}{3}$	-26.860	24.654	0.858
$\frac{1}{2}$	-24.677	17.275	0.499
1	-23.589	9.177	0.255
2	-39.544	8.153	0.288
3	-53.311	7.446	0.348
4	-66.687	7.004	0.402

Table 5: Ra=10^6; h=1/96, dt=0.00001: Various quantities

A	ψ^{min}	$\overline{N}u$	T_{ss}
$\frac{1}{4}$	-29.244	30.845	1.004
$\frac{1}{3}$	-26.924	24.093	0.775
$\frac{1}{2}$	-24.702	16.856	0.531
1	-23.617	8.933	0.271
2	-39.577	7.983	0.304
3	-53.368	7.325	0.366
4	-66.687	7.004	0.403

the basic mesh size $h = \frac{1}{64}$, given in Table 4, can be chosen as representatives to describe the flow.

Table 6: Ra=10^5; h=1/24, dt=0.0001: Various quantities

A	ψ^{min}	$\overline{Nu}$	T_{ss}
$\frac{1}{3}$	-15.650	12.042	1.247
$\frac{1}{2}$	-14.532	8.81	0.849
1	-13.478	4.946	0.428
2	-21.589	4.627	0.514
3	-30.060	4.319	0.59

Table 7: Various Ra's with $A = 1$

Ra	ψ^{min}	T_{ss}	$\overline{Nu}$	$\overline{Nu}_{Vd}$
10^6	-23.589	0.255	9.064	9.035
10^7	-42.603	0.169	20.015	*
10^5	-13.478	0.428	4.946	4.716

iv) In order to make a comparison about the behavior of the flow as Ra increases, Table 6 displays the characteristics of the flow for $Ra = 10^5$ with various aspect ratios A and Table 7 for $Ra = 10^6$ and 10^7 with $A = 1$, supplemented with some characteristics for $Ra = 10^5$, some of them already displayed in Table 6; it must be noted in passing that the results in Table 6 for $Ra = 10^5$, contrary to the results in Tables 4 and 5, were obtained with the basic mesh size $h = \frac{1}{24}$ and $\Delta t = 0.0001$.

Then, with all the above information at hand, we may say that the characteristics of the flow depend on either as Ra increases or as the aspect ratio varies in the following way:

A) With $A = 1$ and varying Ra, Table 7: $|\psi^{min}|$ and the global Nusselt number $\overline{Nu}$ increase, and T_{ss} decreases, as Ra increases. Table 7, last two columns, also shows that the increase of $\overline{Nu}$ agrees with the increase of $\overline{Nu}_{Vd}$, within the most close mesh size, given in De Vahl Davis (1983), where $*$ means that such value is not reported; in connection with this and with Table 6, for $Ra = 10^5$, $\overline{Nu}_{Vd} = 4.716$.

B) For $Ra = 10^6$ fixed and varying A, Table 4: $|\psi^{min}|$ and T_{ss} increase as either A decreases from 1 to $\frac{1}{4}$ or A increases from 1 to 4, and the global Nusselt number $\overline{Nu}$ decreases as A increases from $\frac{1}{4}$ to 4; it must be noted that $|\psi^{min}|$ increase more when A increases from 1 to 4 than when A decreases from 1 to $\frac{1}{4}$, $\overline{Nu}$ increases more when A decreases from 1 to $\frac{1}{4}$ than what it decreases when A increases from

1 to 4, and T_{ss} increases more when A decreases from 1 to $\frac{1}{4}$ than what it increases when A increases from 1 to 4. Qualitatively speaking all these features occur with the finer mesh in Table 5 and in Table 6 for $Ra = 10^5$.

C) On the other hand, let us see the congruence of the local Nusselt number $Nu(y)$ with respect to $\overline{Nu}$ in A) and B): In A), Figure 3 shows that the graph of $Nu(y)$ for $Ra = 10^7$ is above the one of $Ra = 10^6$, then $\overline{Nu}$, given by integral of $N(y)$ on the same interval, must be bigger for $Ra = 10^7$; this relation, not shown here, also holds for $Ra = 10^6$ and $Ra = 10^5$. In B), Figure 6 shows that $Nu(y)$ is not decreasing as A varies from 2 to 4, then $\overline{Nu}$ must increase since the interval of integration also increases; the graph of $Nu(y)$ in Figure 10 has a relation similar to the one in Figure 3 as A decreases from $\frac{1}{2}$ to $\frac{1}{4}$, then $\overline{Nu}$ must increase. About the maximum value of $Nu(y)$ and how close to $y = 0$ is reached are self-explanatory in Figures 3, 6 and 10, which tell us where the maximum heat transfer occurs. Moreover, that the maximum of $Nu(y)$ when A decreases from $\frac{1}{2}$ to $\frac{1}{4}$ be significant bigger, above 35 in Figure 10, than when A increases from 2 to 4, below 23 in Figure 6, implies that $\overline{Nu}$ must be bigger in the first situation, as it has already been stated before.

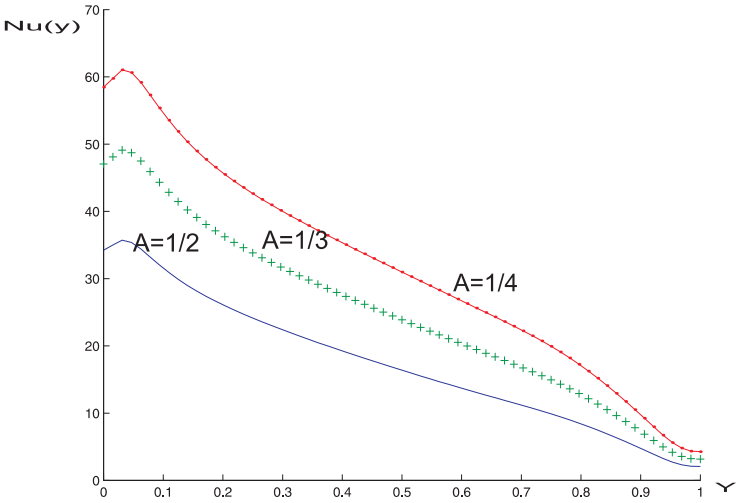

Figure 10: Local Nusselt Number for $Ra = 10^6$: $A = \frac{1}{2}, \frac{1}{3}, \frac{1}{4}$

Last but not least, in connection with the analogous study in Saeid and Pop (2004) for flows in porous media, for $Ra = 10^6$ with $A = 1$ a sequence of results are shown at different times T's before the time when the steady state is reached, given by

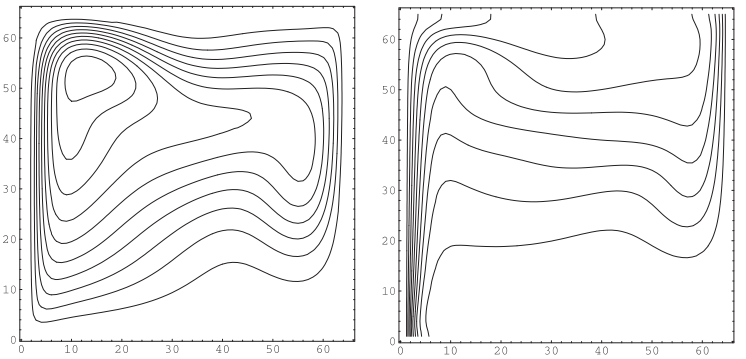

Figure 11: $Ra = 10^6$: $T = 0.016$, streamlines (left), isotherms (right)

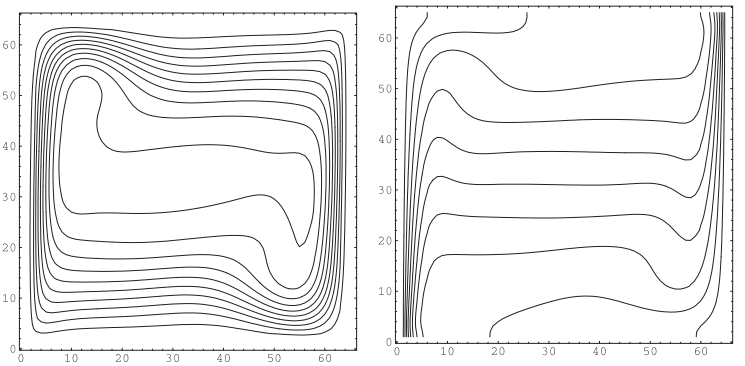

Figure 12: $Ra = 10^6$: $T = 0.064$, streamlines (left), isotherms (right)

$T_{ss} = 0.255$ in Table 4. To this end, Figures 11, 12, and 13 display respectively the flow, streamlines (left) and isotherms (right), at times $T = 0.016$, 0.064, and 0.128 which correspond approximately to $\frac{1}{16}$, $\frac{1}{4}$, and $\frac{1}{2}$ of T_{ss}; it is pointed out that the flow at $\frac{3}{4}$ of T_{ss} looks the same as the one at $\frac{1}{2}$ of T_{ss} in Figure 13. The contour values of the isotherms, as before, vary from 0.09 to 0.9; about the contour values of the stream function we have: in Figure 11, they vary from -3, the closest one to the boundary, to -30, the innermost streamline, we recall that -3 is -30 divided by 10, as it was explained before; in Figure 12 they vary from -2.1 to -21; in Figure 13 they vary also from -2.1 to -21, which are the same at the bigger time $\frac{3}{4}$ of T_{ss}, and surprisingly they are the same at T_{ss}, as it was commented on the description of Figure 1.

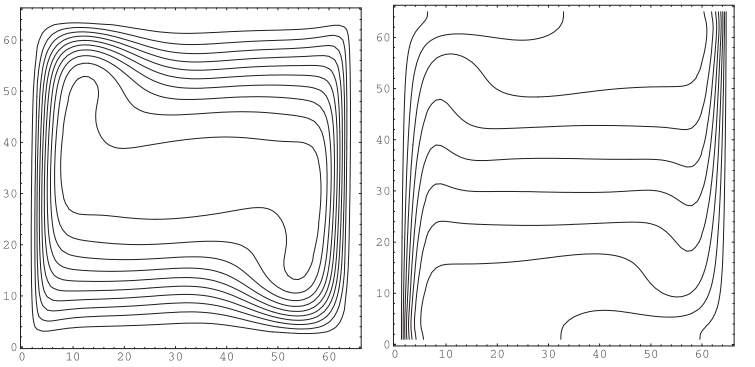

Figure 13: $Ra = 10^6$: $T = 0.128$, streamlines (left), isotherms (right)

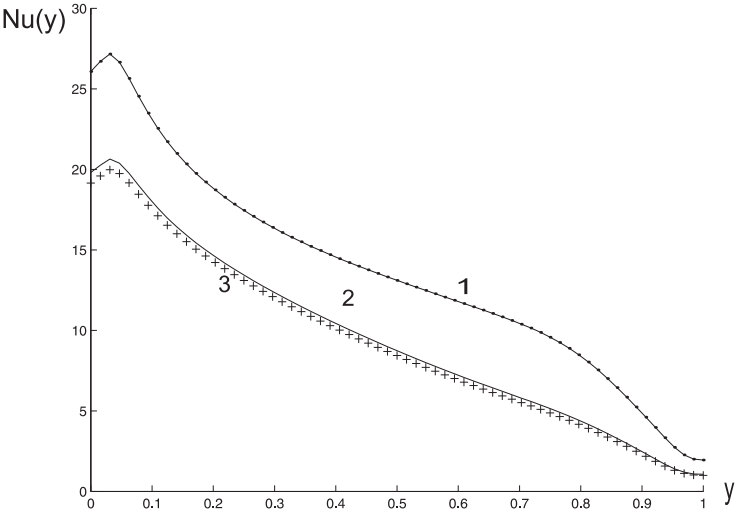

Figure 14: Local Nusselt Number for $Ra = 10^6$: $T = 0.016$ (1), 0.064 (2) and 0.128 (3)

On the other hand, the isotherms in Figure 11 show that, little time after the heating begins, the hot fluid that rises from the bottom, and close to the hot left wall, has spread to occupy more than the upper half of the cavity; at the same time, the streamlines show a recirculation of the flow almost on the same part of cav-

ity starting close to the upper corner. At a later time, Figure 12, the isotherms show that practically the whole fluid has been warmed up, ascending near the hot left wall to the top and falling, by cooling, towards the bottom near the cold right wall (less warm than the fluid). The streamlines equally indicate that the flow has been extended throughout the cavity; although the intensity of its motion has been diminished as the contour values of the streamlines indicate. At a time latter, Figure 13, the flow already exhibits all the characteristics that will be preserved up to $T_{ss} = 0.255$.

The heat transfer along the hot wall, measured through the local Nusselt number, for these three times, is displayed in Figure 14; the respective graphics indicate that the heat transfer at any time is higher in the low part of the hot wall and it diminishes towards the high part of this wall. This agrees very well with the fact that the isotherms are closer each other at the low part of the hot left wall which indicates a higher variation of the temperature, in the horizontal direction, and they are more separated about the end of the wall, as Figures 11, 12 and 13 show. Moreover, since the initial temperature is zero, the heat transfer is greater at a time near zero and diminishes as time increases, as it can be seen in Figure 14, because as long as the temperature of the fluid increases its difference with the hot wall diminishes. It can also be observed in Figure 14 that the smallest difference between the graphics corresponds to the times $\frac{1}{4}$ and $\frac{1}{2}$ of T_{ss}, and the graphics for later times are equal to the one at $\frac{1}{2}$ of T_{ss}. The respective values of the global Nusselt number, at the times we are discussing on, are given by $\overline{Nu}$=13.689, 9.499, 9.186, and at $\frac{3}{4}$ of T_{ss} is given by 9.177; they are reinforcing what it was commented previously: they diminish and tend to the respective value $\overline{Nu}$=9.177 at T_{ss}. Then, the local and global Nusselt numbers are tending, from above, to the ones given at T_{ss}, Table 4 and Figure 3. Clearly this is another source of validation of the flow for $Ra = 10^6$ with A=1; a notorious findings here are: the convergence of these thermal characteristics of the flow to those at T_{ss} is monotone, from above, and like what it occurs in porous media, Saeid and Pop (2004), the characteristics on the motion, and other thermic ones, that are preserved start about $\frac{1}{2}$ of T_{ss}.

4 Conclusions

2D numerical results on natural convection have been presented to study the effects on the characteristics of flows as some parameters, the Rayleigh number Ra and the aspect ratio A of a cavity, vary. The results are obtained with a numerical method previously reported for mixed convection to solve the unsteady Boussinesq approximation in stream function and vorticity variables. The validation of the results is carried out through mesh size and time-step independence studies complemented with the corresponding independence of some parameters of the flow; in this way, the validation process is not depending on the comparison with other works that

use other dimensionless forms. The effects on the characteristics are considered for flows converging to a steady state as Ra and A vary in the range $10^5 \leq Ra \leq 10^7$ and $\frac{1}{4} \leq A \leq 4$, in cavities filled with air. For the dimensionless form we are considering our systematic study on such effects on the characteristics of the flows shows several aspects on the motion and on the heat transfer, given by the Nusselt numbers, which are worth to be considered at the end of the transient stage and even during such stage as it is shown by the study of the case for $Ra = 10^6$ with $A = 1$. For instance, for the former case, the activity of the flow is stronger, motion and global heat transfer, as long as Ra increases since $|\psi^{min}|$ and the global Nusselt number $\overline{Nu}$ increase but the flow reaches its steady state faster since T_{ss} decreases; for the latter case, at times during the transient stage the convergence of some thermal characteristics of the flow to those at T_{ss} is not oscillatory but monotonic. From this study several guidelines are at hand to make an analogous study for higher Ra's and bigger or smaller A's. Previous results for higher Ra's, with A within the same range that is considered here, show a significant restriction on the mesh size and the time step: a finer mesh size and a smaller time step have to be used; besides, it seems that some of these flows appear to be time-dependent which leads to long time computations. Other source of research is to consider a smaller Ra and A large enough, tall cavities, to make a study in connection with cat's eyes.

References

Adams J., Swarztrauber P. and Sweet R. (1980): FISHPACK: A Package of Fortran Subprograms for the Solution of Separable Elliptic PDE's', *The National Center for Atmospheric Research*, Boulder, CO, USA.

Arefmanesh A., Najafi M., and Abdi H. (2008): Meshless Local Petrov-GalerkinMethod with Unity Test Function for Non-Isothermal Fluid Flow. *CMES: Computer Modeling in Engineering and Sciences*, vol.25, no.1, 9-22.

Atluri, S.N., Sladek, J, and Soric, J. (2009): Advances in the MLPG Method. Tech Science Press (in press).

Atluri S. N., Liu H. T., Han Z. D. (2006): Meshless Local Petrov-Galerkin (MLPG) Mixed Finite Difference Method for Solid Mechanics. *CMES: Computer Modeling in Engineering and Sciences*, 15, no. 1, 1-16.

Atluri S. N., Liu H. T., Han Z. D. (2006): Meshless local Petrov-Galerkin (MLPG) mixed collocation method for elasticity problems. *CMES: Computer Modeling in Engineering and Sciences*, 14, no. 3, 141-152.

Atluri, S.N. (2005): *Methods of Computer Modeling in Engineering & the Sciences, Volume 1*. Tech Science Press.

Atluri, S.N. (2004): *The Meshless Method (MLPG) for Domain & Bie Discretiza-*

tions. Tech Science Press.

Atluri, S.N., and Shen S. (2002): *The Meshless Local Petrov-Galerkin (MLPG) Method*. Tech Science Press.

Atluri, S.N., and Zhu, T. (1998): A New Meshless Local Petrov-Galerkin (MLPG) Approach in Computational Mechanics. *Computational Mechanics*, Vol.22, pp. 117-127.

Avila, R., and Solorio, F. J. (2009): Numerical Solution of 2D Natural Convection in a Concentric Annulus with Solid-Liquid Phase Change. *CMES: Computer Modeling in Engineering and Sciences*, vol.44, no.2, pp.177-202.

Báez E., Nicolás A. (2006): 2D natural convection flows in tilted cavities: porous media and homogeneous fluids. *Int. J. of Heat and Mass Transfer*, vol. 49, 4773-4785.

Bourantas, G. C., Skouras E. D., and G. C. Nikiforidis, G.C. (2009): Adaptive Support Domain Implementation on the Moving Least Squares Approximation for Mfree Methods Applied on Elliptic and Parabolic PDE Problems Using Strong-Form Description. *CMES: Computer Modeling in Engineering and Sciences*, vol.43, no.1, pp.1-25.

De Vahl Davis G. (1983): Natural Convection of air in a square cavity: a bench mark numerical solution. *Int. J. Numer. Methods Fluids*, vol. 3, 249-264.

Gunzburger M. D. (1989): *Finite Element Methods for Viscous Incompressible Flows: A guide to theory, practice, and algorithms*. Academic Press, INC.

Glowinski R. (2003): *Hanbook of Numerical Analysis: Numerical Methods for Fluids* (Part 3), North-Holland Ed.

Ho-Minh D., Mai-Duy N. and Tran-Cong T. (2009): A Galerkin-RBF Approach for the Streamfunction-Vorticity-Temperature Formulation of Natural Convection in 2D Enclosured Domains. *CMES: Computer Modeling in Engineering and Sciences*, vol. 44, no. 3, 219-248.

Kosec G. and Ŝarler B. (2008): Local RBF Collocation Method for Darcy Flow. *CMES: Computer Modeling in Engineering and Sciences*, vol. 25, no. 3, 197-207.

Landau L. D., Lifshitz E. M. (1989): *Fluid Mechanics*, Pergamon Press, INC.

Le Quéré P., Alziary de Roquefort T. (1985): Computation of Natural Convection in Two-Dimensional Cavities with Chebyshev Polynomials. *J. of Computational Physics*, vol. 57, 210-228.

Li, S.; Atluri, S. N. (2008): The MLPG mixed collocation method for material orientation and topology optimization of anisotropic solids and structures. *CMES: Computer Modeling in Engineering and Sciences* 30, no. 1, 37-56.

Marin L. (2008): The Method of Fundamental Solutions for Inverse Problems Associated with the Steady-State Heat Conduction in the Presence of Sources. *CMES: Computer Modeling in Engineering and Sciences* 30, no. 2, 99-122.

Nicolás A., Bermúdez B. (2005): 2D Thermal/Isothermal Incompressible Viscous Flows. *Int. J. for Num. Meth. in Fluids*, vol. 48, 349-366.

Nicolás A., Bermúdez B. (2004): 2D Incompressible Viscous Flows at Moderate and High Reynolds Numbers. *CMES: Computer Methods in Engineering and Sciences*, vol. 16, no. 5, 441-451.

Nicolás A., Bermúdez B. (2007): Viscous Incompressible Flows by the Velocity-Vorticity Navier-Stokes Equations. *CMES: Computer Methods in Engineering and Sciences*, vol. 20, no. 2, 73-83.

Peyret R., Taylor T. D. (1983): *Computational Methods for Fluid Flow*, Springer-Verlag, NY.

Rico-García E., Lopez-Cruz I. L., Herrera-Ruiz G., Soto-Zarazúa G. M., Castañeda-Miranda R. (2008): Effect of Temperature on Greenhouse Natural Ventilation under Hot Conditions: Computational Fluid Dynamics Simulations. *Journal of Applied Sciences*, vol. 8, no. 24, 4543-4551.

Saeid N. H., Pop I. (2004): Transient free convection in a square cavity filled with porous medium. *Int. J. of Heat and Mass Transfer*, vol. 47, 1917-1924.